Nanoscale

Accepted Manuscript

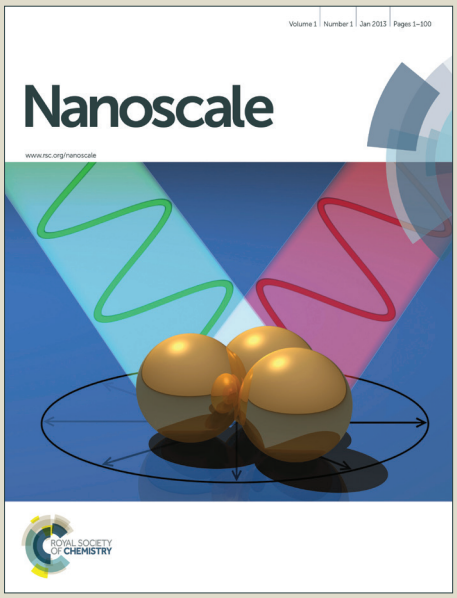

ROYAL SOCIETY OF CHEMISTRY

www.rsc.org/nanoscale

From Graphene Oxide to Pristine Graphene: Revealing the Inner Workings of the Full Structural Restoration

View Article Online
DOI: 10.1039/C4NR05816J

Rubén Rozada, Juan I. Paredes, María J. López, Silvia Villar-Rodil*, Iván Cabria, Julio A. Alonso, Amelia Martínez-Alonso, Juan M. D. Tascón

R. Rozada, Dr. J. I. Paredes, Dr. S. Villar-Rodil, Prof. A. Martínez-Alonso, Prof. J. M. D. Tascón

Instituto Nacional del Carbón, INCAR-CSIC, Apartado 73, 33080 Oviedo, Spain

E-mail: UUsilvia@incar.csic.es

Dr. M. J. López, Dr. I. Cabria, Prof. J. A. Alonso

Departamento de Física Teórica, Atómica y Óptica, Universidad de Valladolid, 47011 Valladolid, Spain

DOI: 10.1039/C4NR05816J

Abstract

High temperature annealing is the only method known to date that allows a complete repair of the defective lattice of graphenes derived from graphite oxide, but most relevant aspects of such restoration process are poorly understood. Here, we investigate both experimentally (scanning probe microscopy) and theoretically (molecular dynamics simulations) the thermal evolution of individual graphene oxide sheets, which is rationalized on the basis of the generation and dynamics of atomic vacancies in the carbon lattice. For unreduced and mildly reduced graphene oxide sheets, the amount of generated vacancies was so large that they disintegrated at 1773-2073 K. By contrast, highly reduced sheets survived annealing and their structure could be completely restored at 2073 K. For the latter, a minority atomic-sized defect with six-fold symmetry was observed and ascribed to a stable cluster of nitrogen dopants. The thermal behavior of the sheets was significantly altered when they were supported onto a vacancy-decorated graphite substrate, as well as for overlapped/stacked sheets. In these cases, a net transfer of carbon atoms between neighboring sheets via atomic vacancies takes place, affording additional healing process. Direct evidence of sheet coalescence with the step edge of the graphite substrate was also gathered from experiments and theory.

INTRODUCTION

Due to a combination of unsurpassed physical properties (e.g., electronic, mechanical, thermal and optical), it is generally agreed that graphene possesses a strong potential to become a key material in many relevant technological applications.[1,2] For example, this strictly two-dimensional, sp^2-hybridized carbon material and some of its derivatives are being extensively investigated towards their use in high frequency transistors,[3] transparent conducting electrodes,[4] energy conversion and storage devices,[5] mechanically reinforced polymer composites,[6] catalytic materials[7] and biomedical systems (drug delivery, imaging, etc.),[8] among other possibilities.

An obvious and necessary condition to the widespread implementation of graphene in such applications is the availability of cost-effective methods for the large-scale production of this

View Article Online
DOI: 10.1039/C4NR05816J

material with characteristics that can be tailored to the specific intended use. To this end, significant research efforts have been directed over the last years to the development of both bottom-up and top-down synthesis approaches.[9,10] The former include most significantly chemical vapor deposition of hydrocarbons onto suitable transition metal substrates (nickel, copper),[11] whereas the latter are mainly focused on the processing of either pristine graphite or graphite oxide by different means.[12,13] The so-called graphite oxide route to graphene has been particularly rewarding not only in terms of bulk production at an affordable cost, but also concerning other features that have a direct bearing on practical issues, such as the colloidal processability of the obtained material in aqueous and organic media or its ease of combination with other materials to form composites and hybrids.[10,14]

The main attraction of graphite oxide as a precursor to graphene lies in the fact that this derivative of graphite, as opposed to the case of its pristine counterpart, can be readily exfoliated to give single layer sheets (graphene oxide sheets), with a subsequent reduction step designed to remove the oxygen functional groups that heavily decorate the carbon skeleton of graphene oxide. Although the resulting product (referred to as reduced graphene oxide) as well as graphene oxide itself have become important materials on their own merit,[15] this approach has traditionally suffered from a significant limitation that hinders its wider utility in the graphene field: the apparent inability of the known reduction methods to fully convert graphene oxide back to pristine graphene. Indeed, virtually all the reduction methodologies that have been reported to this day, including those of chemical, electrochemical, thermal (up to moderately high temperatures) and catalytic nature, have yielded products that retain a significant amount of oxygen and structural defects, the presence of which degrades many of the exceptional properties of graphene.[16,17] To overcome this problem, alternative strategies aimed at the repair of defects in graphene oxide/reduced graphene oxide by the external supply of carbon atoms (chemical vapor deposition techniques) have been explored, but they have met with limited success.[18-20]

View Article Online
DOI: 10.1039/C4NR05816J

In this context, it has become increasingly apparent that high temperature (≥1773 K) heat treatment, i.e. graphitization, is probably the only effective way to achieve a thorough conversion of graphene oxide/reduced graphene oxide to graphene sheets of the highest structural quality. Indeed, recent work by several groups has demonstrated a dramatic decrease in the amount of structural defects and residual oxygen after subjecting reduced graphene oxide samples to graphitization treatments.[21-25] Nevertheless, such studies were conducted either on bulk powders[21-24] or on macroscopically assembled films,[23,25] which probably precluded the observation of many relevant processes taking place upon thermal annealing that can only be investigated and understood by the scrutiny of individual sheets under certain controlled conditions. More specifically, a number of fundamental questions concerning the high–temperature evolution of graphene oxide and reduced graphene oxide sheets have not yet been addressed, including the following: (1) Is it possible to convert a (reduced) graphene oxide sheet to pristine, completely defect-free graphene by heat treatment? If this is the case, what is the temperature required for it to happen? (2) How does the presence (amount) of oxygen functional groups grafted on the carbon skeleton of graphene oxide affect its thermal evolution? (3) What is the effect of other heteroatoms that may be present on graphene oxide (e.g., nitrogen) on its propensity to be healed? (4) Because the sheets need to be typically supported on a substrate, how do the characteristics of the substrate (e.g., inert vs. reactive) influence the thermal evolution of the sheets? (5) How do neighboring sheets interact with each other during the high temperature annealing?

To seek answers to these questions, in the work reported here we have carried out a combined experimental and theoretical study on the structural evolution of graphene oxide and reduced graphene oxide sheets upon graphitization treatments. Nanometer- and atomic-scale imaging of individual sheets or assemblies of a few sheets by scanning tunneling and atomic force microscopy (STM/AFM), together with molecular dynamics simulations, revealed a wealth of new information on the basic processes underlying the healing of the carbon lattice in this graphene derivative. In addition to illuminating the thermal behavior of graphene oxide/reduced graphene oxide materials,

the knowledge generated by the present results should be useful in assisting the design of improved thermal routes to their structural restoration.

View Article Online
DOI: 10.1039/C4NR05816J

EXPERIMENTAL SECTION

Preparation of unreduced and chemically reduced graphene oxide sheets

Unreduced graphene oxide sheets as well as graphene oxide sheets chemically reduced to different degrees, obtained from the processing of graphite oxide, were used for the graphitization experiments. To this end, graphite oxide was prepared from natural graphite powder (Fluka 50870) by the Hummers method using H_2SO_4, $NaNO_3$ and $KMnO_4$.[26] Following a purification step that involved washing first with 10% HCl solution and then with copious amounts of Milli-Q water, the oxidized product was suspended in water, bath-sonicated (J.P. Selecta Ultrasons system, 40 kHz) for 2 h and finally centrifuged (Eppendorf 5424 microcentrifuge) at 10000 *g* for 10 min to sediment unexfoliated graphite oxide particles. The top ~75% of the resulting supernatant volume, which is a colloidal dispersion of unreduced graphene oxide sheets, was collected and kept for further use. The concentration of graphene oxide in this suspension was determined by UV-vis absorption spectroscopy as described elsewhere.[27] An aqueous dispersion of mildly reduced graphene oxide sheets was prepared by heating its unreduced counterpart (concentration ~0.1 mg mL^{-1}) at 368 K for 4 h in the presence of 26 mM ammonia. Similarly, an aqueous dispersion of highly reduced graphene oxide sheets was obtained by heating the unreduced suspension at 368 K for 1 h in the presence of both 26 mM ammonia and 1 mM hydrazine monohydrate. The role of ammonia is to provide a basic medium (pH ~10) that (i) confers colloidal stability to the sheets through electrostatic repulsion and (ii) induces a limited reduction of graphene oxide, probably by way of nucleophilic attack from the hydroxide anions.[28,29] On the other hand, hydrazine is a powerful reducing agent and thus affords a more extensive reduction of the graphene oxide sheets.[28,30]

DOI: 10.1039/C4NR05816J

Thermal annealing experiments

For the graphitization experiments, the sheets need to be deposited onto suitable substrates that, among other requirements, are thermally stable up to very high temperatures. This prerequisite severely constrains the range of substrate materials that can be used, with HOPG being probably the most attractive option in the present case. In addition to its extreme heat resistance, HOPG provides a versatile supporting surface that is mostly atomically flat and inert in its pristine form but can be made atomically rough and reactive through appropriate surface treatment. Here, both pristine (inert) and surface-treated (reactive) HOPG substrates were used. The former were prepared just by cleaving HOPG pieces (grade ZYA, obtained from Tectra GmbH) with adhesive tape, whereas the latter were produced by means of dielectric barrier discharge (DBD)-generated air plasma treatment of the HOPG surface according to a procedure that has been described in detail elsewhere.[31] Briefly, freshly cleaved HOPG pieces were exposed to DBD-generated air plasma in a volume type apparatus (VB-A4, from Arcotec GmbH) at a power of 200 W for 0.35 s. This treatment leads to HOPG surfaces uniformly decorated with a high density of atomic vacancies, the carbon atoms alongside the vacancies constituting locally reactive sites on account of their dangling bonds.[31] The different unreduced and chemically reduced graphene oxide sheets were deposited on either pristine or plasma-treated HOPG substrates by drop-casting a small volume (~5 μL) of their corresponding diluted suspension (~0.01-0.02 mg mL^{-1}) onto the substrate pre-heated at ~323-333 K and allowing it to dry. These samples were subsequently introduced in a graphite furnace and heat treated at a given (target) temperature under continuous argon flow (2 L min^{-1}). For reasons that will be commented upon below, the range of target temperatures investigated here was between 1773 and 2273 K. The following heating rates were applied: 50 K min^{-1} from room temperature to 973 K, 100 K min^{-1} from 973 to 1273 K, 25 K min^{-1} from 1273 K up to the target temperature, then constant target temperature for 60 min and finally cooling down to room temperature.

View Article Online
DOI: 10.1039/C4NR05816J

Characterization techniques

Morphological and structural characterization of the heat-treated graphene oxide/reduced graphene oxide sheets on the nanometer and atomic scales was carried out by STM and AFM. To this end, a Nanoscope IIIa Multimode apparatus (Veeco Instruments) working under ambient conditions (relative humidity ~40%, temperature ~295-297 K) was used. STM imaging was accomplished in the constant current mode (variable height) using mechanically prepared Pt/Ir tips with typical tunneling parameters of 5-1500 mV (bias voltage) and 0.1-3 nA (tunneling current). AFM was performed in the tapping mode of operation using silicon cantilevers (spring constant ~40 N m^{-1}, resonance frequency ~250-300 kHz). Information on some aspects of the chemistry of the sheets (non-graphitized and graphitized) was obtained by means of XPS and TPD. Macroscopic, free-standing paper-like films of the sheets assembled via vacuum filtration of their corresponding aqueous dispersion were used as specimens for XPS and TPD rather than the HOPG substrates loosely decorated with the sheets that were employed for STM and AFM. Such films were subjected to the same annealing procedures as those applied to the HOPG-supported sheets. The XPS measurements were carried out in a SPECS system working at a pressure below 10^{-7} Pa with a monochromatic Al Kα X-ray source (100 W). TPD profiles were recorded with a Micromeritics Autochem II chemisorption analyzer at a heating rate of 10 K min^{-1} under Ar flow (50 mL min^{-1}). CO and CO_2 evolution was quantitatively determined from the intensity of *m/z* = 28 and 44, respectively, as measured by an Ommistar mass spectrometer (Pfeiffer Vacuum).

Theoretical modeling

Molecular dynamics simulations were performed to attain further insight into several aspects of the annealing process. The simulations were focused on reduced graphene oxide sheets supported onto reactive graphite substrates, more specifically (i) a graphite surface decorated with atomic vacancies and (ii) a step edge on an otherwise pristine graphite surface, where interlayer interactions promoted by these defects are to be expected. Because heat treatment of reduced graphene oxide removes all

View Article Online
DOI: 10.1039/C4NR05816J

residual oxygen groups and generates unsaturated atomic vacancies (see Results and discussion section), the simulations began at the point where the vacancies had been created and no oxygen groups were present in the sheets. The graphite substrate with the reduced graphene oxide sheet was mimicked by a slab of five graphitic layers. The simulations were performed using periodic boundary conditions in the graphitic planes (XY plane) and free conditions in their perpendicular direction (Z direction). The supercell in the XY plane contained 12×16 rectangular unit cells of graphene with size $\left(\sqrt{3}r_0, 3r_0\right)$, where r_0 is the carbon-carbon bond length in graphite and each unit cell contains four carbon atoms. Thus, a perfect layer of graphene contains 768 carbon atoms within the supercell. The bottom layer of the slab had a perfect, defect-free structure and was kept rigid during the simulations to represent the bulk of graphite for the remaining four layers. Four atoms at the edge of the supercell were also fixed in each of the 3 topmost layers to keep the layers bound to the graphitic surface even at the highest temperatures in the simulations. The slab was allowed to evolve dynamically at several temperatures. The interaction between carbon atoms was mimicked through a computationally efficient many-body empirical potential[32] that represents the carbon-carbon covalent bonds in graphite and diamond through a short-range Tersoff-like potential[33,34] and incorporates a long-range many-body potential[35] to represent weak van der Waals interactions between layers in graphite. This potential has proved to be reliable in the description of a wide variety of carbon systems, including fullerenes,[32] carbon nanotubes[36,37] or carbide-derived carbons.[38] The interatomic Tersoff potential gives a melting temperature for carbon of about 6000 K, whereas the experimental value is about 4300 K. Therefore, the temperatures given in this paper have been scaled by a factor of 0.7. The simulations were performed at constant number of particles and constant temperature, using the Nose-Hoover thermostat. The equations of motion were solved with a time step of 0.5 fs.

RESULTS AND DISCUSSION

View Article Online
DOI: 10.1039/C4NR05816J

General thermal behavior of unreduced and chemically reduced graphene oxide sheets at high temperature

To provide the conceptual starting point and rationale for the investigations reported here, some general considerations about the known structure and thermal behavior of graphene oxide need to be taken into account. First, previous work has determined that the carbon skeleton in graphene oxide sheets is heavily decorated by epoxide and hydroxyl functional groups on their basal plane, whereas a minority of other functionalities (carboxyls, carbonyls, etc) can be found at the sheet edges.[39-41] This picture is in great contrast with that of most carbon materials, where virtually all the oxygen-containing functional groups are located at the sheet edges.[42] The spatial distribution of the oxygen groups in graphene oxide is locally inhomogeneous: isolated domains of essentially intact, defect-free graphene a few nanometers in lateral size are surrounded by strongly oxidized, predominantly sp^3-based areas where the epoxides and hydroxyls are concentrated.[43] Chemical reduction protocols (e.g., using hydrazine) typically remove most of the oxygen functionalities on the basal plane, so that the pristine graphene domains become larger, more numerous and interconnected in the reduced sheets.[43] It is noteworthy that chemical reduction in these conditions does not eliminate the oxygen functionalities located at the sheet edges, so that the carbon atoms at the edges are not expected to be saturated with hydrogen. Second, a large fraction of the oxygen functional groups in graphene oxide decompose by thermal annealing in a narrow range of low temperatures (~398-473 K) to yield mainly CO and CO_2 molecules, though a steady and slower CO/CO_2 evolution is observed up to at least 1273 K.[44,45] This thermal behavior differs significantly from that of typical carbon materials, which usually undergo high temperatures during the processes involved in their natural genesis or their synthetic preparation, and thus possess more stable oxygen functionalities, which evolve at temperatures above 473 K.[42,46] Following a heat treatment at such moderately high temperatures (~1273-1373 K), the carbon sheets still retain a non-negligible

View Article Online
DOI: 10.1039/C4NR05816J

amount of residual, apparently quite stable oxygen groups.[47-49] This behavior has been qualitatively accounted for on the basis of recent theoretical simulations:[50,51] the very high local density of oxygen groups in graphene oxide promotes concerted reactions that favor, both kinetically (low activation barrier) and thermodynamically, the dissociation of many of these groups to yield CO/CO_2 molecules together with atomic vacancies in the carbon lattice. The formed carbon vacancies are rapidly saturated by some of the remaining oxygen to give, e.g., carbonyl or ether groups, which are very stable and can only be dissociated by overcoming a high energy barrier (high activation temperature).[50,51]

The previous considerations indicate that after annealing at moderately high temperatures (up to ~1373 K), the structure of the original graphene oxide/reduced graphene oxide sheets evolves into one dominated by (probably multiatomic) carbon vacancies decorated with stable oxygen groups.[52] Therefore, in the absence of an external supply of carbon atoms that could possibly close the vacancies,[53] further healing of the carbon structure towards a pristine, defect-free graphene sheet should be attained by annealing at higher temperatures to first dissociate the stable oxygen groups and then annihilate the unsaturated carbon vacancies. In this scenario, the amount of oxygen groups present on the sheets prior to their heat treatment should have a strong effect on the subsequent evolution of the carbon structure, because the number of carbon atoms that are removed from the lattice as CO/CO_2, and therefore the number and/or size of the vacancies, must be directly related to the starting oxygen concentration. To investigate this point, graphene oxide sheets with different degrees of reduction (unreduced as well as mildly and highly reduced by chemical means) were deposited onto freshly cleaved highly oriented pyrolytic graphite (HOPG) substrates and first heat-treated at 1773 K. Such particular temperature was chosen because very recent work indicates that it suffices to remove virtually all the oxygen groups from graphene oxide-based films.[25] Thus, no generation of vacancies by CO/CO_2 evolution is expected above this temperature.

Fig. 1a-c shows representative AFM images of the different starting, as-deposited sheets. They all display a similar appearance, i.e., irregular shapes with lateral sizes typically between a few and

View Article Online
DOI: 10.1039/C4NR05816J

several hundred nanometers, and an apparent thickness (determined relative to the HOPG substrate) that in most cases was ~1 nm, indicating that the majority of the sheets are single-layer objects.[27] On the other hand, visible differences were observed in their thermal evolution depending on the reduction degree. The annealing step at 1773 K apparently caused a significant structural deterioration of the unreduced graphene oxide sheets (Fig. 1d), as large unfilled areas (up to a few hundreds of nanometers) of irregular shape and rough boundaries were developed within them (two examples are marked by red arrows in Fig. 1d). Their mildly reduced counterparts better endured the thermal process, although relatively large (tens of nanometers) pits were also seen to develop occasionally (Fig. 1e). By contrast, at this level of magnification in the AFM images, the highly reduced sheets were not seen to undergo any significant morphological changes (Fig. 1f) apart from a decrease in their apparent thickness, which was also observed for the unreduced and mildly reduced sheets. This thickness closely approached the value for single-layer, pristine graphene (~0.34 nm; see overlaid line profiles in Fig. 1d-f). Because the sheets were supported on the surface of a substrate (as-cleaved HOPG) that is chemically and structurally identical to perfect graphene, the AFM-derived thickness values are consistent with the idea that all these sheets have undergone extensive deoxygenation.[54]

Annealing at higher temperatures further accentuated the differences between sheets reduced to different extents. For example, heat treatment at 2073 K led to the disintegration of the unreduced graphene oxide sheets as only some disjoined fragments were left on the HOPG surface (Fig. 1g). The mildly reduced sheets experienced a lesser, but still considerable, level of disintegration as the sheets preserved in the sample were rather scarce and showed smaller sizes after the heat treatment (Fig. 1h). On the contrary, their highly reduced counterparts survived the annealing process without any apparent sign of deterioration (Fig. 1i). At such annealing temperature, the contour of the sheets become noticeable rounded, which is thought to be a result of the high mobility of the carbon atoms at the sheet edges.[55]

View Article Online
DOI: 10.1039/C4NR05816J

We interpret that in the case of unreduced graphene oxide (Fig. 1a,d and g), a very large fraction of carbon atoms are removed as CO and CO_2 from the lattice during the thermal annealing, in particular from the highly oxidized regions where the oxygen functional groups are clustered. Because the highly oxidized regions originally formed a continuous, percolated network in between intact graphene domains,[43] it is plausible that the number of carbon atoms left behind in such regions upon heat treatment is too low to be able to strongly hold the intact graphene domains together. As a result, the latter can easily detach from the sheets at the high annealing temperatures, thus giving rise to unfilled areas within the sheets at 1773 K (Fig. 1d) and to their disintegration at higher temperatures (Fig. 1g). This idea is supported by the presence of remains of the small fragments that agglomerate at the boundaries of these areas (e.g. see red arrows in Fig. 1d). Indeed, detachment of minute graphene domains (<10 nm) from this type of graphene derivative has been previously observed in a somewhat different context (oxidation and etching processes at lower temperature).[56] For mildly reduced graphene oxide (Fig. 1b, e and h), the highly oxidized regions should be smaller and probably not so well interconnected, so a better endurance is envisaged in this case, but in any event the number of atomic vacancies that are thermally generated should still be relatively high. These vacancies can migrate and coalesce to form larger vacancies, so nanometer-sized pits would initially appear (Fig. 1e), and eventually a higher degree of damage would be generated upon further coalescence processes (Fig. 1h). Finally, in the case of highly reduced graphene oxide (Fig. 1c, f and i), relatively little oxygen is present and therefore a small number of vacancies will be thermally produced, which is not sufficient to create nanometer-sized pits in the sheets.

To gain an approximate idea of the amount of vacancies that are involved in each of the three scenarios described in Fig. 1, we note that the fraction of carbon atoms thermally removed from the graphene oxide/reduced graphene oxide lattice can be quantitatively estimated on the basis of the amount of CO and CO_2 evolved from the samples, as measured by temperature programmed desorption (TPD), together with the information on their elemental composition that can be

View Article Online
DOI: 10.1039/C4NR05816J

obtained by X-ray photoelectron spectroscopy (XPS). The results are given in Table 1. It should be stressed that the calculated percentage of thermally removed carbon atoms most probably underestimates the actual values for the three samples. The reason is connected to the fact that the amount of evolved CO and CO_2 was measured only up to 1273 K due to limitations of the TPD apparatus. However, because the large majority (>80%) of the oxygen functional groups are removed in this temperature range,[47-49] the values provided in Table 1 should be fairly close to the real ones and therefore can be considered reasonable estimates. As could be expected, the (global) fraction of carbon atoms removed from unreduced graphene oxide is quite high (~ 28%), but locally it should be even higher in the heavily oxidized areas of the sheets. Such result lends support to the idea that only very loose connections between the intact graphene domains remain upon the heat treatment, thus facilitating the development of unfilled areas and the eventual disintegration of the sheets (Fig. 1d and g). On the other hand, it appears that the carbon lattice can withstand abstraction of about 4% of its atoms and still be healed without developing large and/or irreversible morphological changes (Fig. 1f).

Achieving full structural restoration of individual, chemically reduced graphene oxide sheets: thermal evolution of atomic-scale defects

The previous results suggest that only graphene oxide sheets that have undergone considerable reduction by chemical means, a process not believed to be associated to significant carbon atom abstraction,[57-59] can be eventually healed through heat treatment, at least in the case of isolated sheets on the inert, atomically flat HOPG substrate. The unreduced sheets are damaged when their oxygen functionalities are completely stripped off, whereas mildly reduced graphene oxide develops pits that are too large to be eliminated at higher temperatures. For this reason, hereupon we will exclusively focus on aspects of the thermal behavior of the highly reduced sheets.

As noted above, when all the oxygen is eliminated from a sheet at a sufficiently high temperature (~1773 K),[25] the generated atomic vacancies will probably become mobile and start

View Article Online
DOI: 10.1039/C4NR05816J

diffusing across the sheet. The diffusion of a given vacancy can be expected to proceed until either (1) it is annihilated at the edge of the sheet, thus effectively healing the defect, or (2) it bumps into another vacancy, coalescing with it and forming a larger, more stable vacancy.[60] Obviously, to achieve full structural restoration of the sheet, event (1) must dominate over event (2) in the long run, but this should only be possible when the fraction of carbon atoms that were removed from the lattice is sufficiently small. Otherwise, the probability of vacancy coalescence would be very high, giving rise to large-sized vacancies. Taking into account that the mobility of a vacancy is expected to decrease with its size (for instance, the migration barrier for a monovacancy is 1.2-1.4 eV, but already 5-7 eV for a divacancy),[61,62] if the size of the coalesced vacancies becomes too large, their mobility will be severely reduced, which effectively inhibits their annihilation. On the other hand, when the vacancy size and density are kept below a certain level, efficient annihilation processes, and consequently an extensive restoration of the sheet, should be possible.

To investigate this question in the case of highly reduced graphene oxide, the sheets that had been heat treated at 1773 K were examined in more detail by STM, a technique that is well known to allow visualization of atomic vacancies and other point defects on graphitic surfaces.[31] Representative nanometer and atomic scale images for this sample are shown in Fig. 2c and d, respectively. For comparison, STM images of the starting, non-annealed sheets recorded at the same levels of magnification are also given (Fig. 2a and b). The latter display an atomically rough morphology on the nanometer scale (Fig. 2a) and a highly distorted, non-periodic structure on the atomic scale (Fig. 2b), which is consistent with the presence of residual oxygen groups and a locally strained carbon lattice, as expected for highly reduced graphene oxide.[27] Heat treatment at 1773 K brought about significant changes to the sheets, although it did not fully repair their structure: the morphology of the sheets was dominated by a large number of randomly scattered bright features (i.e. apparent protrusions) with somewhat ill-defined boundaries on the nanometer scale (Fig. 2c). The protrusions were approximately between 2 and 5 nm in lateral size and exhibited distorted patterns on the atomic scale, whereas the flat areas in-between displayed an essentially well-

View Article Online
DOI: 10.1039/C4NR05816J

ordered, graphitic structure (Fig. 2d). Such characteristics are consistent with the basic hypothesis that heat treatment of the sheets generates a carbon structure decorated by atomic vacancies: it is well established that an atomic vacancy in graphite/graphene is imaged by STM as an apparent protrusion by virtue of an enhancement in the local density of electronic states near the Fermi level in the region surrounding the vacancy.[63-66] We therefore ascribe the protrusions seen in Fig. 2c and d to the atomic vacancies created in the sheets by the heat treatment. Furthermore, such features most probably correspond to multiatomic vacancies rather than monatomic ones, as the latter have been shown to be associated to smaller protrusions (~1 nm).[66] Due to the very high density of vacancies in the sample, individual protrusions were in many cases difficult to clearly make out in the nanometer-scale images (Fig. 2c), which thus tended to be visualized as slightly blurred features with ill-defined boundaries.

To probe the subsequent evolution of the vacancies, annealing experiments at increasingly higher temperatures were conducted and the resulting samples inspected again by STM: representative images are shown in Fig. 2e and f (1923 K), g and h (2073 K), and i and j (2223 K). Following heat treatment at 1923 K, a high density of protrusions was again observed, in this case ~3-5 nm wide (Fig. 2e). Although at first sight there were no drastic differences between this sample and the one annealed at 1773 K, a closer look revealed a subtle but unequivocal change, i.e., the protrusions in the former appeared to be more isolated and sharply defined features (compare Fig. 2e with c). We attribute this change to an overall decrease in the vacancy density due to the annihilation and/or coalescence of a fraction of those vacancies originally present in the sheets heat-treated at 1773 K, which became sufficiently mobile when the temperature was increased to 1923 K. On the other hand, after annealing at 2073 K (Fig. 2g and h) the ~3-5 nm wide protrusions disappeared completely and the sheets developed an essentially pristine structure with long-range graphitic order that was only locally broken by the presence of small protrusions of uniform size (~1-1.5 nm), which were finally removed at 2223 K (Fig. 2i and j). Although such result demonstrates that a full recovery of the graphene lattice can be attained between 2073 and 2223 K,

View Article Online
DOI: 10.1039/C4NR05816J

it also challenges the implicit assumption that atomic vacancies are the only type of defect present in the highly reduced sheets upon thermal removal of their oxygen groups. If smaller vacancies can be associated to smaller STM protrusions and higher mobilities[61-66] and the ~1-1.5 nm wide protrusions were indeed atomic vacancies (probably monatomic ones, according to their size),[66] then the latter should not have survived the annealing process after all the larger vacancies (protrusions) were annihilated. On the contrary, they should have been the first to be annihilated. We therefore have to conclude that these small protrusions are not atomic vacancies but a different type of defect. Moreover, virtually all the protrusions remaining in the 2073 K sample exhibited a six-fold symmetry (Fig. 2h) that has never been reported for atomic vacancies (either monatomic or multiatomic) in graphitic materials. We stress that such characteristic is not the result of a tip artefact, as different STM tips consistently yielded the very same pattern. This also indicates that only one type of defect is present in the sheets following treatment at 2073 K. It is likewise worth noting that some ~1-1.5 nm wide protrusions could already be observed in the sheets annealed at 1923 K, but their proximity to larger protrusions did not allow their unambiguous identification as independent, stand-alone defects.

We believe that the small, symmetrical protrusions reflect the presence of some substitutional nitrogen species in the carbon lattice. First, the reduced graphene oxide used here was prepared with hydrazine as a reductant in the presence of ammonia, a process that is known to introduce nitrogen species on the sheets (see XPS data in Table 1).[30] Second, XPS provided evidence that some of this nitrogen survives heat treatment at high temperatures: survey spectra of reduced graphene oxide films annealed at 1773 K (not shown) revealed an amount of nitrogen close to the detection limit of the technique (~0.2 at%), but nonetheless still noticeable. In addition, the high resolution N1s spectrum of these films (Fig. 3) was dominated by a component at about 401.6 eV, which can be assigned to quaternary nitrogen in a graphitic lattice.[67,68] A smaller component observed at ~399.2 eV was attributed to pyridinic nitrogen, which is presumed to be located at the edge of the vacancies. It would thus not be unreasonable that a small fraction of such substitutional nitrogen

View Article Online
DOI: 10.1039/C4NR05816J

still survives annealing at 2073 K. No nitrogen was detected by XPS for films heat treated at 2073 K, but this result could be anticipated due to the low density of protrusions (~4×10^3 μm^{-2}) seen by STM on the corresponding sheets (Fig. 2g). If we assume that every protrusion pinpoints the position of one or just a few nitrogen atoms, this element would be present in a proportion of the order of 0.01 at%, which is below the detection limit of XPS. Third, recent experimental and theoretical work has shown that substitutional nitrogen dopants in graphene/graphite transfer a fraction of their extra electron to their neighboring carbon atoms, so that this type of defect is visualized by STM as a small (< 2 nm) apparent protrusion.[69-71] More specifically, for a single substitutional nitrogen dopant the associated STM protrusion has been shown to display a trigonal symmetry that was not observed in the present case. Still, more complex symmetrical patterns have also been observed in nitrogen-doped graphene and attributed to small nitrogen dopant clusters of unidentified configuration.[69] It is therefore plausible that the six-fold symmetrical features reported here correspond to some specific type of dopant cluster, in particular one that seems to be especially stable.

A control experiment was carried out by which reduction of the graphene oxide was accomplished using vitamin C in place of hydrazine/ammonia. This treatment leads to the same extent of reduction as achieved with hydrazine, but is not expected to introduce nitrogen species.[28] We observed the same evolution of protrusions ~2-5 nm large in the 1773-2073 K temperature range as described above for the hydrazine-reduced sheets. However, in this case no small-sized bright features were observed upon annealing at 2073 K, i.e. the sheets were completely defect free, suggesting that such features are indeed associated to nitrogen species. They also indicate that introduction of nitrogen, at least at concentrations of a few at%, does not significantly influence the ultimate thermal evolution of the sheets, as full repair of the carbon structure is achieved at 2073-2223 K both in the presence and absence of nitrogen. This result seems to be different to that observed when the sheets are just annealed at lower temperatures: a recent report has suggested that

View Article Online
DOI: 10.1039/C4NR05816J

nitrogen introduced via hydrazine reduction favors the development of a somewhat less defected carbon structure at temperatures below 1373 K compared to sheets without nitrogen species.[72]

Influence of substrate defects and sheet-sheet interactions on the thermal evolution of chemically reduced graphene oxide sheets

The previous results on the thermal evolution of unreduced/chemically reduced graphene oxide were focused on isolated sheets supported onto the atomically flat and defect-free terraces of pristine HOPG. Under such conditions, it is reasonable to assume that there is a weak interaction between the sheets and the inert substrate, and therefore their thermal behavior will not be significantly affected by the latter. For example, it is not expected that atomic vacancies will migrate from the sheets to the pristine HOPG terrace: the activation energy for this process is estimated to be already as high as ~8 eV for a monatomic vacancy[73] and should be much higher for multiatomic ones, which would effectively prevent it from taking place. Nevertheless, in the presence of substrate defects or for stacked/overlapped/folded sheets this behavior might be altered as a result of interlayer interactions promoted by the defects. To investigate this point, three different situations were contemplated: (1) isolated sheets covering two neighboring pristine terraces across a step edge, (2) overlapped sheets supported onto a pristine terrace, and (3) isolated sheets supported onto a terrace densely decorated with atomic vacancies. The STM image of Fig. 4a shows an example of the first scenario, in which an individual sheet is seen to cross a monatomic step edge on the pristine HOPG surface. This type of feature was commonly found on account of the relatively small width of the terraces for the HOPG pieces used here (a few micrometers). After heat treatment at 1773 K, it was invariably observed that the lower-lying section of these sheets merged with the upper terrace of the HOPG substrate, leaving their upper-lying section as an isolated entity (Fig. 4b). The unequivocal identification of the merged and isolated sections as arising from the thermal evolution of a given sheet was based on the following observations: (1) both the merged and isolated sections exhibited a large number of nanometer-sized protrusions

View Article Online
DOI: 10.1039/C4NR05816J

(e.g., Fig. 4c and d), indicating the generation of atomic vacancies that is characteristic of the annealed sheets; (2) merged features were only seen after the heat treatment, but never before; (3) the isolated sections on the upper HOPG terrace were sitting next to the boundary between such terrace and the merged section.

The merging process should be driven by strong interactions between the sheets and the step edges of the HOPG substrate. We interpret that many of the atomic vacancies thermally generated on the sheets will migrate and become pinned at a certain point of an imaginary line defined by the intersection of the sheet with the substrate step edge. Vacancy pinning would be due to formation of covalent bridges between unsaturated carbon atoms from the vacancy and the step edge. If the number of atomic vacancies on the sheets is sufficiently large, then it is plausible that a more or less continuous string of pinned vacancies could develop along this imaginary line. As a result, the linkages between the upper- and lower-lying sections of the sheet would be severely weakened and eventually broken, leading to the coalescence of the latter with the upper terrace of the HOPG substrate. Merging of the upper-lying section of the sheet with the HOPG terrace would be energetically unfavorable due to the high local curvature of the lattice along the seam line. We recently proposed that overlapping sheets in macroscopic, paper-like films of chemically reduced graphene oxide undergo coalescence due to high temperature annealing.[25] However, such phenomenon could not be directly observed and was only inferred on the basis of general morphological changes of the films. The present results (Fig. 4b-d) provide direct evidence that coalescence processes do indeed take place on the sheets at high temperature. However, there is a discrepancy in the actual temperatures required for merging to occur between the isolated sheets on the HOPG step edges (1773 K) and the overlapped sheets in the macroscopic films (at least 2073-2373 K).[25] An explanation for this question will be provided below.

Because the sheets were randomly deposited onto the HOPG surface, they cannot be expected to be exhibit an ordered (AB) stacking registry with the latter, but rather a turbostratic one. This implies that the seam line where the sheet and terrace merge should constitute a grain boundary. In

DOI: 10.1039/C4NR05816J

this type of line defect, the carbon lattice is locally distorted, e.g. by the presence of pentagons and heptagons, giving rise to localization of electronic states near the Fermi level.[74,75] Consequently, grain boundaries in graphitic structures are typically visualized by STM as apparently elevated features,[75,76] and this is indeed what we observed at the seam line where the sheet and the HOPG terrace met (e.g., Fig. 4d-f). The essentially electronic and non-topographic nature of the protruding lines seen here by STM was confirmed by the fact that such lines did not show up in AFM images, which are only sensitive to topography but not to partial electronic density.[77] The presence of a grain boundary-like defect at the seam line is also consistent with the observation that atomic vacancies (protrusions), which were still present on the sheets after coalescence took place at 1773 K, were never seen on the other side of the seam line (e.g, see Fig. 4c and d). Grain boundaries are known to act as vacancy sinks in graphitic systems,[60] and therefore diffusing vacancies can be expected to be annihilated once they reach this type of line defect. Another consequence of the random stacking of the sheets on the HOPG surface was the observation of Moiré patterns, which are superperiodic structures arising from the relative rotation of the two topmost graphene layers.[75] In the present case, such patterns were more easily seen for the highly graphitized sheets (e.g., those annealed at 2073 or 2223 K). An example of a Moiré pattern on a sheet annealed at 2223 K is given in Fig. 4e (bottom left part of the image).

Fig. 5a illustrates the thermal behavior at 1923 K of a sheet folding over itself supported onto the pristine HOPG surface. The most noticeable feature was the development of monolayer-deep pits of nanometric dimensions (~10 nm) in the overlapping region of the sheet, which is reminiscent of the evolution of pits in the mildly reduced sheets reported above. These pits, which start to be discernible at 1773 K (e.g., Fig. 4b), were also observed in overlapping regions involving different sheets but never in non-overlapping/non-folded areas or in isolated sheets (e.g., Fig. 1f). Thus, the generation of pits must be the result of interactions between the two sheets. In principle, the monolayer-deep pits might be located on either of the two sheets, but high resolution STM imaging of the pit edges should enable to determine their actual configuration: if a pit is located on the

View Article Online
DOI: 10.1039/C4NR05816J

topmost sheet, then it should display an atomically sharp edge in the STM images (see upper schematic in Fig. 5b); on the other hand, if the pit was located in the underlying sheet, and therefore covered by the topmost sheet, we would expect to observe a continuous structure with a smoothly decreasing height when going from the edge to the bottom of the pit (Fig. 5b, lower schematic). In the detailed images of the pits shown in Fig. 5c and d, which are representative of all the examined overlapped sheets, it is clear that the pits exhibited atomically sharp edges, hence indicating that they formed only on the topmost sheet. If we assume that pits in this type of graphene sheets are generated when the fraction of carbon atoms missing from their lattice is large enough, then we have to conclude that many more carbon atoms were abstracted from the topmost graphene sheet (in the overlapping/folded area) than expected a priori from their initial oxygen content. We hypothesize that these extra missing carbon atoms were not removed in the form of CO or CO_2, but were directly transferred to the underlying sheet instead.

According to theoretical calculations by different groups,[73,78-81] atomic vacancies from adjacent sheets in graphitic systems can form covalent interlayer bridges with a low energy barrier when they come sufficiently close to each other. Interlayer bonding (i.e., vacancy trapping) is made possible by a displacement of the carbon atoms surrounding the vacancies out of their respective planes of about 0.1 nm.[73,78] With a fraction of thermally removed carbon atoms in the highly reduced sheets of at least 4% (Table 1), vacancy trapping should be a highly probable event when these sheets are stacked over each other. It would then be conceivable that the carbon atoms that participate in the interlayer bonding could leap from one sheet to the other,[81] thereby increasing the vacancy size in the former and decreasing it in the latter. Very recent theoretical modeling has indeed demonstrated that such process, which involves carbon atom displacements of about 0.2 nm, is associated to moderate energy barriers (~3 eV),[82] so it would be readily accessible under the high temperature conditions used here. This carbon atom transfer process is also thermodynamically favorable because larger, coalesced vacancies tend to be more stable than many smaller vacancies with equivalent total number of missing carbon atoms (due to minimization of the energy associated

View Article Online
DOI: 10.1039/C4NR05816J

to dangling bonds).[60,82] However, why we only observe net transfers of carbon atoms from the topmost sheet to its underlying counterpart and not the reverse has to be explained.

The transfer of carbon atoms from the topmost reduced graphene oxide sheet to its underlying counterpart should entail, in addition to the creation of pits in the former, the shrinkage or even disappearance of the vacancies from the latter. Because smaller vacancies possess higher in-plane mobility,[61,62] the logical consequence would be that we observed an improved degree of structural restoration in the underlying sheet in an overlapping area at, e.g., 1923 K compared with the same sheet in their non-overlapping areas or for isolated sheets. Indeed, detailed STM inspection of underlying sheets, which became visible at the bottom of the pits, revealed a much more pristine, less defected structure at 1923 K (i.e., lower density of protrusions, Fig. 5d) than that of the same sheets in non-overlapping areas (images not shown) and isolated sheets annealed at the same temperature (e.g., Fig. 2e). To further demonstrate the involvement of vacancies from adjacent sheets in the observed processes, a further experiment was carried out. Isolated sheets were deposited onto HOPG, the surface of which had been previously decorated with atomic vacancies generated on purpose by plasma treatment (Fig. 5e).[31] A very high density of vacancies was produced exclusively on the topmost layer of the HOPG sample by the bombardment of energetic ions from the plasma, which induced an atomically rough surface morphology (see inset to Fig. 5e).[31] Following heat treatment at 2073 K, a large number of monolayer-deep pits (Fig. 5f) with atomically sharp edges and relatively defect-free bottoms were seen to develop (see inset to Fig. 5f), indicating again that a transfer of carbon atoms, in this case from the sheet to the vacancy-decorated surface of HOPG, took place. This behavior was not observed for the same sheets supported onto pristine HOPG (Fig. 1i).

Further insight into the healing process by molecular dynamics simulations

To provide a deeper understanding of several relevant phenomena described in the previous sections, molecular dynamics simulations of the annealing process were undertaken. We first

View Article Online
DOI: 10.1039/C4NR05816J

investigated the case of a reduced graphene oxide sheet covering two neighboring graphite terraces across a step edge. To simulate a step edge, the surface layer of graphite was replaced by a graphene ribbon of infinite length along the X direction and eight unit cells wide in the Y direction, with zig-zag terminations. This simulation cell thus contained two parallel step edges in the X direction. A reduced graphene oxide sheet was then deposited across the steps. Because our focus was neither on the generation of vacancies in the reduced sheets nor on their diffusion across the sheet, the latter of which has been extensively studied in the literature,[83] we began the simulations at the point where the vacancies had already been created in the sheet and had enough time to diffuse until they became pinned on top of the step edges. Vacancy pinning, i.e. the formation of covalent bridges between the vacancy and the step edge, was indeed observed in our simulations for isolated monatomic vacancies.

The structure of a slab consisting of three complete graphene layers, the ribbon that mimics the step edge and a pristine graphene sheet on top of it was first fully relaxed. We then generated 16 monatomic vacancies on the topmost sheet, i.e., a string of 8 vacancies on top of each step edge (the edge has a length of 12 zig-zag unit cells). This arrangement can be seen in Fig. 6. The temperature of the system was subsequently ramped up, starting at 210 K and increased by 70 K every 10 ps until reconstruction of the structure was observed. We note that the simulation temperatures required to observe the reconstruction of the structure are in general higher than the experimental ones due to the very limited simulation time. In the simulation, once the vacancies are placed in the proximity of the step edge, some of their dangling bonds saturate very fast with some dangling bonds of the edge in less than 1 ps, forming covalent bonds that link the step with the deposited graphene sheet (see Fig. 7). With increasing temperature, more bonds form between the step edge and the lower lying section of the graphene sheet, and bond-forming and bond-breaking events become more frequent. Finally, at 2450 K (after 320 ps), the graphene sheet breaks along a line parallel to the step edge, so that its lower lying section merges with the step, reconstructing a perfect graphene layer, and its upper section is left as an isolated fragment (Fig. 7), in agreement

View Article Online
DOI: 10.1039/C4NR05816J

with the experimental observations described above (Fig. 4). In the simulation, however, because the graphene sheet was deposited in registry with the step, its merged section did not develop any grain boundary at the seam line (Fig. 8).

We also performed simulations of a graphene sheet deposited onto a vacancy-decorated graphite surface, to investigate the role played by interlayer interactions induced by this defect type in the thermal evolution of the sheet. In this case, we considered a graphite slab made up of 5 layers, where the two topmost ones have 60 randomly distributed monatomic vacancies each within the simulation cell. The selected number of vacancies (corresponding to the removal of 8 C at %) is related to the starting oxygen concentration in highly reduced graphene oxide sheets (see Table 1). The three remaining layers are kept defect free. The simulation began at 350 K and the temperature was increased stepwise by 70 K every 1 ps, reaching a final temperature of 3010 K after 39 ps. Snapshots of the simulation are shown in Fig. 9. The carbon atoms around the vacancies have dangling bonds and are very reactive, and exhibited, as expected, a strong tendency to bind to atoms from neighboring layers, preferentially atoms with dangling bonds from vacancies. Thus, a number of covalent bridges were seen to form between the two topmost layers of the system, although a few linkages also formed between the second (vacancy decorated) and third (pristine) layers. These bridges are very efficient in saturating dangling bonds, but are quite costly in energy as compared to pristine graphene. As the simulation temperature is ramped up, bond-forming and bond-breaking events become more frequent, and some of these events give rise to the migration of carbon atoms between neighboring layers. Hence, such events provide a mechanism for the interlayer diffusion and coalescence of vacancies into larger, more energetically stable ones.

However, within the simulation time of 39 ps the number of carbon atoms exchanged between the two topmost layers remains small (about 19), and no net transfer, i.e. neither towards the graphene sheet on the top nor towards the graphite surface underneath, is observed. Moreover, these two layers exhibit a similar distribution of small multiatomic vacancies (see Fig. 9). Therefore, such results are not consistent with the experimental observations described above, where large

View Article Online
DOI: 10.1039/C4NR05816J

vacancies (pits) only formed on the topmost graphene sheet while its underlying substrate was restored. To address this issue, the dynamical simulations were carried on for another 300 ps at a constant temperature of 3010 K. Bond-forming and bond-breaking events continued to provide the mechanism for the interlayer migration of carbon atoms and vacancy coalescence. Nevertheless, for these longer simulation times we observed a preferential migration (i.e., net transfer) of carbon atoms: about 52 atoms migrate from the graphite surface to the graphene sheet placed on top, whereas 108 atoms migrate in the opposite direction, yielding a net transfer of 56 atoms towards the graphite surface. As a consequence, the vacancy-decorated graphite surface is almost completely restored, whereas large multiatomic vacancies (pits) develop in the graphene sheet (Fig. 9). Such results are in agreement with the experiments reported in the previous section.

Concerning the mechanism that drives the net transfer of carbon atoms between the layers, we note that in the hypothetical case of free-standing, unsupported films comprising two or more stacked reduced graphene oxide sheets, the overall probability of carbon atom transfer from a given sheet to an adjacent one should be virtually the same as that of the reverse process. In such a case, no net transfer of carbon atoms between neighboring sheets, but only an enlargement of vacancies via interlayer coalescence processes, should be expected. On the other hand, when the film is supported onto a pristine, defect-free graphite substrate, the latter introduces an asymmetry in the system. Such asymmetry should involve an additional energetic stabilization for carbon atoms that are transferred to the reduced graphene oxide sheet immediately adjacent to the defect-free substrate. This additional stabilization is afforded by the weak, but non-negligible, van der Waals interaction associated to the fully conjugated, pristine graphite substrate, and would drive a net transfer of carbon atoms to this sheet. Indeed, recent calculations have revealed that the formation energy of an atomic vacancy in the bulk of graphite is somewhat larger than that on the graphite surface, suggesting that there is a thermodynamic drive for vacancies to migrate from the bulk to the surface.[73,80] In our case, the simulations indicate that interlayer vacancy (or carbon atom) migration is kinetically enabled by the covalent bridges formed between the vacancies.[81,82]

View Article Online
DOI: 10.1039/C4NR05816J

Regardless of the specific effects associated to the graphite substrate, the formation of covalent bridges (vacancy trapping) between the reduced graphene oxide sheets poses more general implications on their structural restoration. Because vacancy trapping is expected to increase the energy barrier to the in-plane migration of this defect[73,78-80] and the structural restoration of the sheets is thought to ultimately depend on its mobility, we have to conclude that full restoration of a multilayer film should be significantly harder to achieve compared to the restoration of an isolated sheet. The results from the present as well as a previous work[25] indicate that this is indeed the case. For example, atomic vacancies were still present in paper-like films annealed at 2073 K,[25] whereas they were completely removed from isolated sheets (Fig. 2g). Similarly, sheet coalescence, which appears to rely on the in-plane mobility of atomic vacancies (see above), was observed to occur at a lower temperature in isolated sheets compared with multilayer films. Taken together, all these results provide experimental support to the idea proposed by Heggie and co-workers that interlayer bonding via defects should be determinant in the annealing behavior of highly defected graphitic materials.[78]

CONCLUSIONS

We have demonstrated that thermal annealing can convert individual, stand-alone graphene oxide sheets to completely defect-free graphene. Because healing of the sheets is a process dominated by the generation and migration (both intralayer and interlayer) of atomic vacancies in the carbon lattice, their successful restoration at temperatures as low as possible entails the fulfillment of two main requirements: (i) prior to annealing, the amount of oxygen groups on the graphene oxide sheets must be drastically decreased, e.g. by chemical reduction, to limit the thermal evolution of carbon atoms as CO/CO_2 and thus the creation of atomic vacancies, and (ii) the sheets must be supported onto an inert substrate to prevent interactions with the vacancies that could alter their migration dynamics. In those cases where the vacancies from a given sheet strongly interact with

View Article Online
DOI: 10.1039/C4NR05816J

defects from the supporting substrate (e.g., step edges or atomic vacancies in graphite) or from neighboring sheets (stacked/overlapped configurations), the observed annealing behavior is significantly altered, giving rise to coalescence processes, slowed-down vacancy migration and/or carbon atom transfer between adjacent layers. With the graphene oxide sheets used here, which were prepared by standard oxidation protocols, full annihilation of defects could be achieved at 2073 K. However, we envisage that this temperature can be decreased to some extent using much less oxidized forms of graphene oxide, which have been previously reported in the literature. The latter should give rise to thermally induced vacancies of smaller size and/or in lower amounts, which would thus be easier to annihilate.

Acknowledgements

Financial support from the Spanish MINECO and the European Regional Development Fund (projects MAT2011-26399 and MAT2011-22781), as well as from Junta de Castilla y León (grant VA158A11-2) is gratefully acknowledged. R.R. thanks the receipt of a pre-doctoral contract (FPU) from the Spanish MECD.

References

1. A.K. Geim, *Science* 2009, **324**, 1530–1534.
2. K.S. Novoselov, V.I. Fal´ko, L. Colombo, P.R. Gellert, M.G. Schwab and K. A Kim, *Nature* 2012, **490**, 192-200.
3. Y.Q. Wu, Y.M. Lin, A.A. Bol, K.A. Jenkins, F.N. Xia, D.B. Farmer, Y. Zhu and P. Avouris, *Nature* 2011, **472**, 74-78.
4. S. Bae, H. Kim, Y. Lee, X.F. Xu, J.S. Park, Y. Zheng, J. Balakrishnan, T. Lei, H.R. Kim, Y.I. Song, Y.J. Kim, K.S. Kim, B. Özyilmaz, J.-H. Ahn, B.H. Hong and S. Iijima, *Nature Nanotech.* 2010, **5**, 574-578.
5. B. Luo, S.M. Liu and L.J. Zhi,. *Small* 2012, **8**, 630-646.
6. J.R. Potts, D.R. Dreyer, C.W. Bielawski and R.S. Ruoff, *Polymer* 2011, **52**, 5-25.
7. B.F. Machado and P. Serp, *Catal. Sci. Technol.* 2012, **2**, 54-75.

View Article Online
DOI: 10.1039/C4NR05816J

8. H.Y. Mao, S. Laurent, W. Chen, O. Akhavan, M. Imani, A.A. Ashkarra and M. Mahmoudi, *Chem. Rev.* 2013, **113**, 3407–3424.

9. D.R. Dreyer, R.S. Ruoff and C.W. Bielawski, *Angew. Chem. Int. Ed.* 2010, **49**, 9336-9344.

10. S. Guo and S. Dong, *Chem. Soc. Rev.* 2011, **40**, 2644-2672.

11. Y. Zhang, L. Zhang and C. Zhou, *Acc. Chem. Res.* 2013, **46**, 2329–2339.

12. M. Cai, D. Thorpe, D.H. Adamson and H.C. Schniepp, *J. Mater. Chem.* 2012, **22**, 24992-25002.

13. J.N. Coleman, *Acc. Chem. Res.* 2013, **46**, 14-22.

14. O.C. Compton and S.T. Nguyen, *Small* 2010, **6**, 711-723.

15. K.P. Loh, Q. Bao, G. Eda and M. Chhowalla, *Nature Chem.* 2010, **2**, 1015-1024.

16. S. Pei and H.-M. Cheng, *Carbon* 2012, **50**, 3210-3228.

17. S. Mao, H. Pu and J. Chen, *RSC Adv.* 2012, **2**, 2643-2662.

18. V. López, R.S. Sundaram, C. Gómez-Navarro, D. Olea, M. Burghard, J. Gómez-Herrero, F. Zamora and K. Kern, *Adv. Mater.* 2009, **21**, 4683-4686.

19. B. Dai, L. Fu, L. Liao, N. Liu, K. Yan, Y. Chen and Z. Liu, *Nano Res.* 2011, **4**, 434-439.

20. M. Cheng, R. Yang, L. Zhang, Z. Shi, W. Yang, D. Wang, G. Xie, D. Shi and G. Zhang, *Carbon* 2012, **50**, 2581-2587.

21. D. Long, W. Li, W. Qiao, J. Miyawaki, S.-H. Yoon, I. Mochida and L. Ling, *Nanoscale* 2011, **3**, 3652.

22. M. Jin, T.H. Kim, S.C. Lim, D.L. Duong, H.J. Shin, Y.W. Jo, H.K. Jeong, J. Chang, S. Xie and Y.H. Lee, *Adv. Funct. Mater.* 2011, **21**, 3496-3656.

23. T. Ghosh, C. Biswas, J. Oh, G. Arabale, T. Hwang, N.D. Luong, M. Jin, Y.H. Lee and J.-D. Nam, *Chem. Mater.* 2012, **24**, 594-599.

24. Y. Zhang, D. Li, X. Tan, B. Zhang, X. Ruan, H. Liu, C. Pan, L. Liao, T.;Zhai, Y. Bando, S. Chen, W. Cai and R.S. Ruoff, *Carbon* 2013, **54**, 143-148.

25. R. Rozada, J.I. Paredes, S. Villar-Rodil, A. Martínez-Alonso and J.M.D. Tascón, *Nano Res.* **2013**, **6**, 216-233.

26. W.S. Hummers and R.E. Offeman, *J. Am. Chem. Soc.* 1958, **80**, 1339.

27 J.I. Paredes, S. Villar-Rodil, P. Solís-Fernández, A. Martínez-Alonso and J.M.D. Tascón, *Langmuir* 2009, **25**, 5957-5968.

28 M.J. Fernández-Merino, L. Guardia, J.I. Paredes, S. Villar-Rodil, P. Solís-Fernández, A. Martínez-Alonso and J.M.D. Tascón, *J. Phys. Chem. C* **2010**, 114 , 6426-6432

29. A.M. Dimiev, L.B. Alemany and J.M. Tour, *ACS Nano* 2013, **7**, 576-588.

View Article Online
DOI: 10.1039/C4NR05816J

30 D. Li, M.B. Müller, S. Gilje, R.B. Kaner and G.G. Wallace, *Nature Nanotech.* 2008, **3**, 101-105.

31 P. Solís-Fernández, J.I. Paredes, M.J. López, I. Cabria, J.A. Alonso, A. Martínez-Alonso and J.M.D. Tascón, *J. Phys. Chem. C* 2009, **113**, 18719-18729.

32. P.A. Marcos, J.A. Alonso, A. Rubio and M.J. López, *Eur. Phys. J. D* 1999, **6**, 221-233.

33. J Tersoff, *Phys. Rev. B* 1999, **37**, 6991-7000.

34. J. Tersoff, *Phys. Rev. Lett.* 1988, **61**, 2879-2882.

35.K. Nordlund, J. Keinonen and T. Mattila, *Phys. Rev. Lett.* 1996, **77**, 699-702.

36. M.J. López, A. Rubio, J.A. Alonso, L.-C. Qin and S. Iijima, *Phys. Rev. Lett.* 2001, **86**, 3056-3059.

37. M.J. López, A. Rubio, J.A. Alonso, S. Lefrant, K. Méténier and S. Bonnamy, *Phys. Rev. Lett.* 2002, **89**, 255501.

38. M.J. López, I. Cabria and J.A. Alonso, *J. Chem. Phys.* 2011, **135**, 104706.

39. A. Lerf, H. He, M. Forster and J. Klinowski, *J. Phys. Chem. B* 1998, **102**, 4477-4482.

40. T. Szabó, O. Berkesi, P. Forgó, K. Josepovits, Y. Sanakis, D. Petridis and I. Dékány, *Chem. Mater*. 2006, **18**, 2740-2749.

41. W. Cai, R.D. Piner, F.J. Stadermann, S. Park, M.A. Shaibat, Y. Ishii, D. Yang, A. Velamakanni, S.J. An, M. Stoller, J. An, D. Chen and R.S. Ruoff, *Science* 2008, **321**, 1815-1817.

42. J.L. Figueiredo, M.F.R. Pereira, M.M.A. Freitas, J.J.M. Órfão, *Carbon* 1999, **37**, 1379–1389.

43. K. Erickson, R. Erni, Z. Lee, N. Alem, W. Gannett and A. Zettl, *Adv. Mater*. 2010, **22**, 4467-4472.

44. I. Jung, D.A. Field, N.J. Clark, Y. Zhu, D. Yang, R.D. Piner, S. Stankovich, D.A. Dikin, H. Geisler, C.A. Ventrice and R.S. Ruoff, *J. Phys. Chem*. C 2009, **113**, 18480-18486.

45. P. Solís-Fernández, R. Rozada, J.I. Paredes, S. Villar-Rodil, M.J. Fernández-Merino, L. Guardia, A. Martínez-Alonso and J.M.D. Tascón, *J. Alloys Compd*. 2012, **536S**, S532-S537.

46 U. Zielke, K.J. Huttinger, W.P. Hoffman, *Carbon* 1996, **34**, 983–998.

47. C. Mattevi, G. Eda, S. Agnoli, S. Miller, K.A. Mkhoyan, O. Celik, D. Mastrogiovanni, G. Granozzi, E. Garfunkel and M. Chhowalla, *Adv. Funct. Mater*. 2009, **19**, 2577-2583.

48. O. Akhavan, *Carbon* 2010, **48**, 509-519.

49. C.-M. Chen, Q. Zhang, M.-G. Yang, C.-H. Huang, Y.-G. Yang, M.-Z. Wang, *Carbon* 2012, **50**, 3572-3584.

50. A. Bagri, C. Mattevi, M. Acik, Y.J. Chabal, M. Chhowalla and V.B. Shenoy, *Nature Chem.* 2010, **2**, 581-587.

View Article Online
DOI: 10.1039/C4NR05816J

51. T. Sun, S. Fabris and S. Baroni, *J. Phys. Chem. C* 2011, **115**, 4730-4737.

52.G. Lee, K.S. Kim and K. Cho, *J. Phys. Chem. C* 2011, **115**, 9719-9725.

53. L. Liu, K.T. Rim, D. Eom, T.F. Heinz and G.W. Flynn, *Nano Lett.* 2008, **8**, 1872-1878.

54. P. Solís-Fernández, J.I. Paredes, S. Villar-Rodil, A. Martínez-Alonso and J.M.D. Tascón, *Carbon* 2010, **48**, 2657-2660.

55. C.Ö. Girit, J.C. Meyer, R. Erni, M.D. Rossell, C. Kisielowski, L. Yang, C.-H. Park, M.F. Crommie, M.L. Cohen, S.G. Louie and A. Zettl, *Science* 2009, **323**, 1705-1708.

56. P. Solís-Fernández, J.I. Paredes, S. Villar-Rodil, L. Guardia, M.J. Fernández-Merino, G. Dobrik, L.P. Biró, A. Martínez-Alonso and J.M.D. Tascón, *J. Phys. Chem. C* 2011, **115**, 7956-7966.

57. S. Stankovich, D.A. Dikin, R.D. Piner, K.A. Kohlhaas, A. Kleinhammes, Y.Y. Jia, Y. Wu, S.T. Nguyen and R.S. Ruoff, *Carbon* 2007, **45**, 1558-1565.

58. M.C. Kim, G.S. Hwang and R.S. Ruoff, *J. Chem. Phys.* 2009, **131**, 064704.

59. X.F. Gao, J. Jang and S. Nagase,. *J. Phys. Chem. C* 2010, **114**, 832-842.

60. F. Banhart, *Rep. Prog. Phys.* 1999, **62**, 1181-1221.

61. F. Banhart, J. Kotakoski and A.V. Krasheninnikov, *ACS Nano* 2011, **5**, 26-41.

62. J.Y. Huang, F. Ding and B.I. Yakobson, *Phys. Rev. B* 2008, **78**, 155436.

63. J.R. Hahn and H. Kang, *Phys. Rev. B* 1999, **60**, 6007-6017

64. A.V. Krasheninnikov, K. Nordlund, M. Sirviö, E. Salonen and J. Keinonen, *J. Phys. Rev. B* 2001, **63**, 245405.

65. H. Amara, S. Latil, V. Meunier, Ph. Lambin and J.-C. Charlier, *Phys. Rev. B* 2007, **76**, 115423.

66. J.I. Paredes, P. Solís-Fernández, A. Martínez-Alonso and J.M.D. Tascón, *J. Phys. Chem. C* 2009, **113**, 10249-10255.

67. S. Kundu, W. Xia, W. Busser, M. Becker, D.A. Schmidt, M. Havenith and M. Muhler, Phys *Phys. Chem. Chem. Phys.* 2010, **12**, 4351-4359.

68. H. Wang, T. Maiyalagan and X. Wang, *ACS Catal.* 2012, **2**, 781-794.

69. L. Zhao, R. He, K.T. Rim, T. Schiros, K.S. Kim, H. Zhou, C. Gutiérrez, S.P. Chockalingam, C.J. Arguello, L. Pálová, D. Nordlund, M.S. Hybertsen, D.R. Reichman, T.F. Heinz, P. Kim, A. Pinczuk, G.W. Flynn and A.N. Pasupathy, *Science* 2011, **333**, 999-1003.

70. F. Joucken, Y. Tison, J. Lagoute, J. Dumont, D. Cabosart, B. Zheng, V. Repain, C. Chacon, Y. Girard, A.R. Botello-Méndez, S. Rousset, R. Sporken, J.-C. Charlier and L. Henrard, *Phys. Rev. B* 2012, **85**, 161408.

71. T. Kondo, S. Casolo, T. Suzuki, T. Shikano, M. Sakurai, Y. Harada, M. Saito, M. Oshima, M.I. Trioni, G.F. Tantardini and J. Nakamura, *Phys. Rev. B* 2012, **86**, 035436.

72. Y. Yoon, S. Seo, G. Kim and H. Lee, *Chem. Eur. J.* 2012, **18**, 13466-13472.

73.G. Teobaldi, K. Tanimura and A.L. Shluger, *Phys. Rev. B* 2010, **82**, 174104.

74. S. Kurasch, J. Kotakoski, O. Lehtinen, V. Skákalová, J. Smet, C.E. Krill, A.V. Krasheninnikov and U. Kaiser, *Nano Lett.* 2012, **12**, 3168-3173.

75. H.S. Wong, C. Durkan and N. Chandrasekhar, *ACS Nano* 2009, **3**, 3455-3462.

76. P. Simonis, C. Goffaux, P.A. Thiry, L.P. Biró, P. Lambin and V. Meunier, *Surf. Sci.* 2002, **511**, 319-322.

77.S .N. Magonov, M.-H. Whangbo, Surface Analysis with STM and AFM, VCH: Weinheim, 1996.

78. R.H. Telling, C.P.Ewels, A.A. El-Barbary and M.I. Heggie, *Nature Mater.* 2003, **2**, 333-337.

79. A.A. El-Barbary, R.H. Telling, C.P. Ewels, M.I. Heggie and P.R. Briddon, *Phys. Rev. B* 2003, **68**, 144107.

80. G. Teobaldi, H. Ohnishi, K. Tanimura and A.L. Shluger, *Carbon* 2010, **48**, 4145-4161.

81. T. Trevethan, P. Dyulgerova, C.D. Latham, M.I. Heggie, C.R. Seabourne, A.J. Scott, P.R. Briddon and M.J. Rayson, *Phys. Rev. Lett.* 2013, **111**, 095501.

82. L. Liu, J. Gao, X. Zhang, T. Yan and F. Ding, *Nanoscale* 2014, **6**, 5729-5734.

83. G.-D. Lee, C.Z. Wang, E. Yoon, N.-M. Hwang, D.-Y. Kim and K.M. Ho, *Phys. Rev. Lett.* 2005, **95**, 205501.

Table 1 Atomic composition calculated from XPS spectra and amount of CO and CO_2 released during TPD up to 1273 K for graphene oxide and reduced graphene oxide paper-like films.

Sample	Atomic composition by XPS (at. %)			Species released by TPD (mmol g^{-1})		Fraction of carbon atoms removed (%)
	C	O	N	CO	CO_2	
Unreduced graphene oxide	70.4	29.1	0.5	8.3	6.1	28
Mildly reduced graphene oxide	74.9	22.1	3.0	2.0	4.4	11
Highly reduced graphene oxide	90.1	8.1	1.8	1.4	1.9	4

View Article Online
DOI: 10.1039/C4NR05816J

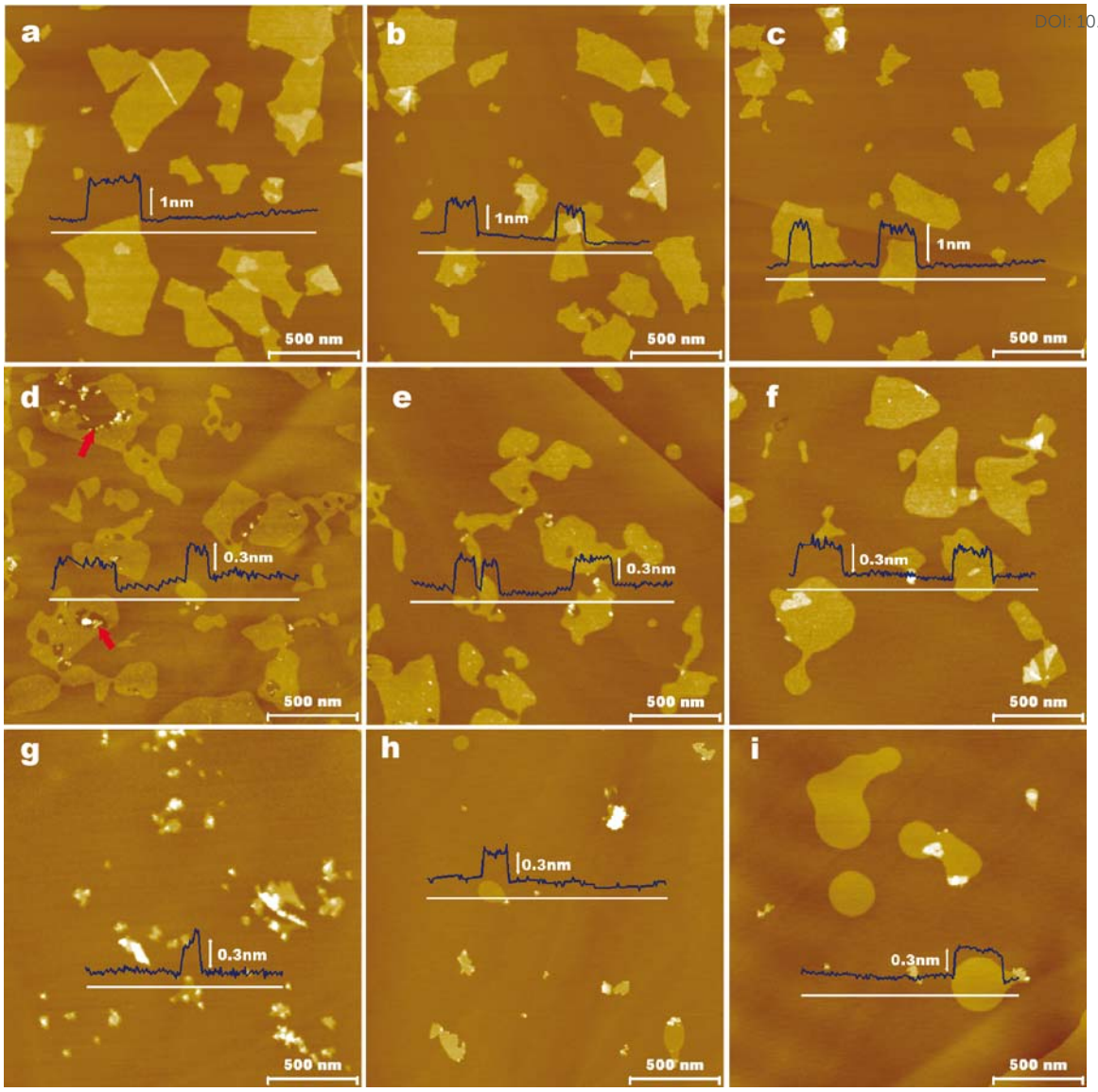

Figure 1 Nanometer-scale AFM images for the unreduced (a,d,g), mildly reduced (b,e,h) and highly reduced (c,f,i) graphene oxide sheets deposited on top of a HOPG substrate, prior to the thermal treatment (a-c) and annealed at 1773 K (d-f) and 2073 K (g-i).

View Article Online
DOI: 10.1039/C4NR05816J

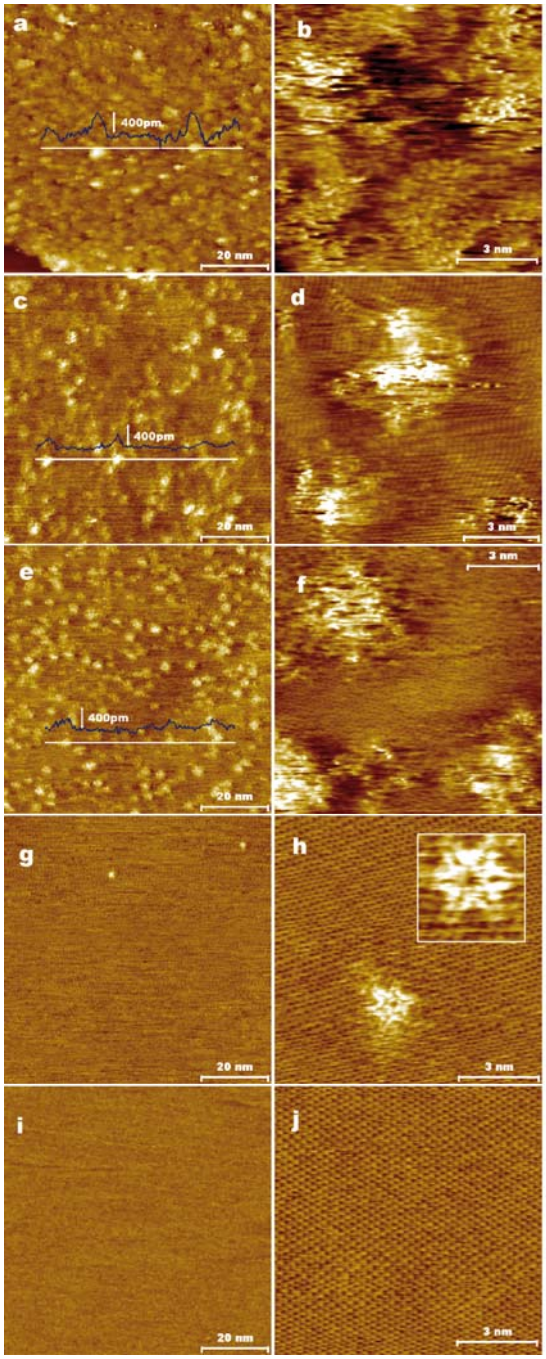

Figure 2 Nanometer- and atomic-scale STM images for the highly reduced graphene oxide sheets prior to the thermal treatment (a,b) and after annealing at 1773 K (c,d), 1923 K (e,f), 2073 K (g,h) and 2223 K (i,j). The inset to (h) is a detailed 2x2 nm^2 image showing a different image of the same type of defect. Imaging conditions: 0.3 nA (tunneling current) and 500mV (bias voltage) (a,c,e,g,i); 1-4 nA and 5-10mV (b,d,f,j); 0.5 nA and 80mV (h); 0.8nA and 50mV (inset).

View Article Online
DOI: 10.1039/C4NR05816J

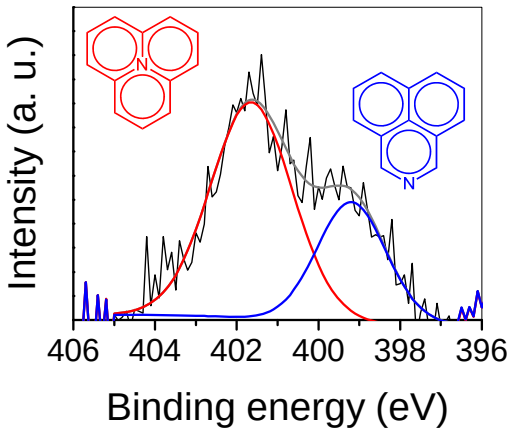

Figure 3 High resolution N1s core level XPS spectrum of the sample treated at 1773 K (black line), together with its deconvolution into two components at 401.6 eV (red line) and 399.2 eV (blue line), which are assigned to quaternary and pyridinic nitrogen, respectively. The corresponding envelope is included (grey line)

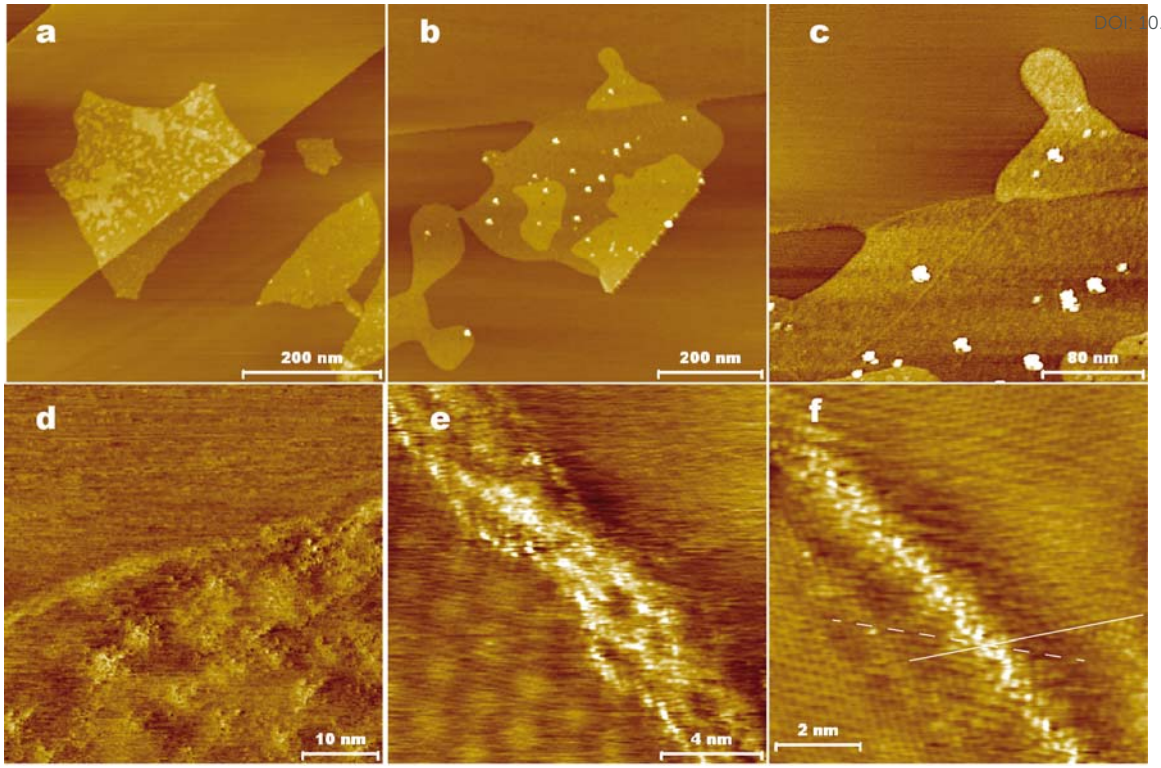

Figure 4 Nanometer-scale STM image of highly reduced graphene oxide sheets deposited on top of a HOPG substrate, showing an individual sheet covering two neighboring pristine terraces across a monatomic step edge, prior to the heat-treatment (a) and after annealing at 1773 K (b,c,d). Atomic-scale STM images of a Moiré Pattern (e) and a grain boundary (e,f) in highly reduced graphene oxide sheets annealded at 2223 K. Imaging conditions: 0.1-0.7 nA (tunneling current) and 300-1500 mV (bias voltaje) (a,b,c,d); 2nA and 5mV (e,f).

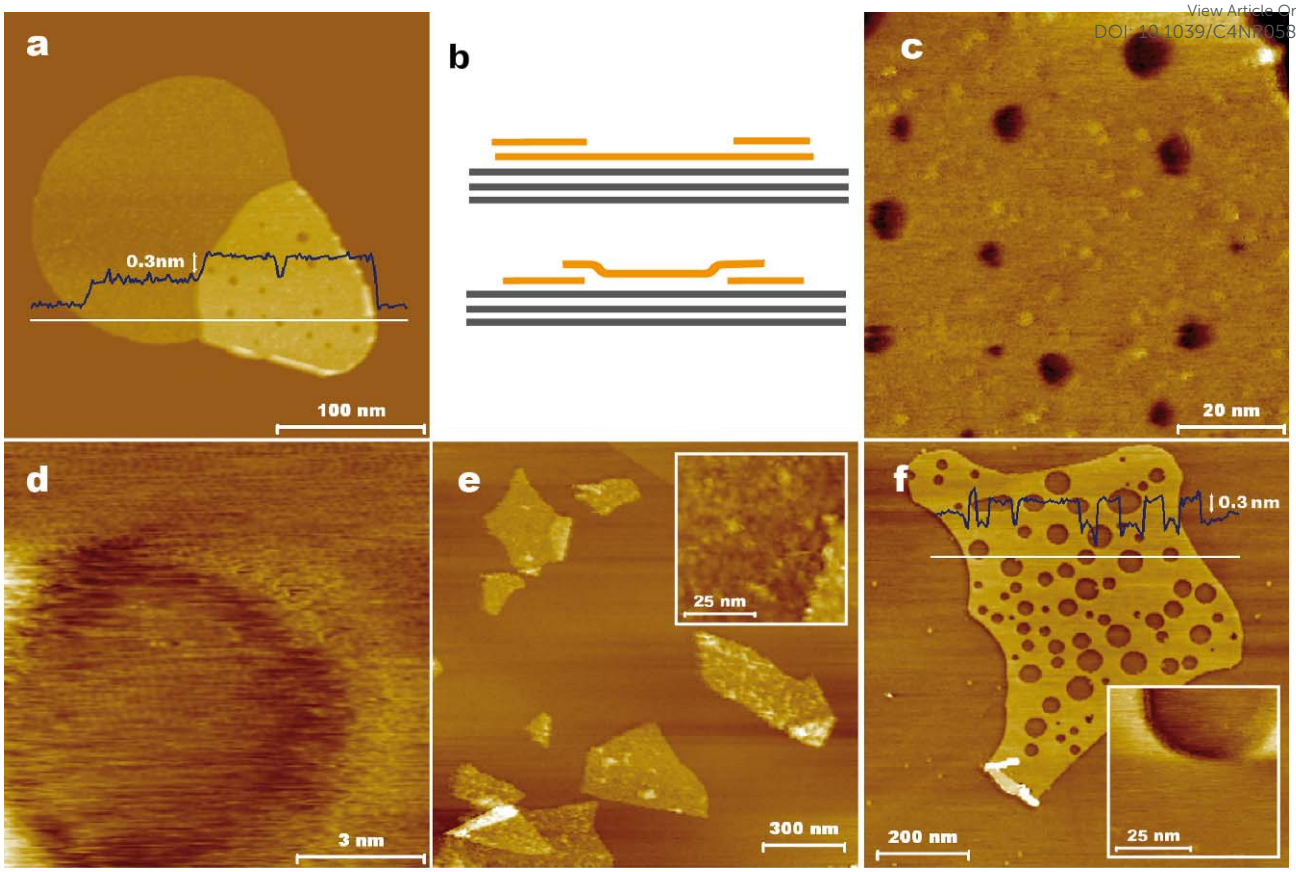

Figure 5 Nanometer-scale STM image of a highly reduced graphene oxide sheet folding over itself supported onto the pristine HOPG surface after annealing at 1923 K (a). Schematic illustration of the possible configurations of a pit in the region of overlapping of highly reduced graphene oxide sheets (b). Nanometer-scale (c) and atomic-scale (d) STM images of the region of overlapping shown in (a). Nanometer-scale image of highly reduced graphene oxide sheets deposited on top of a HOPG substrate previously exposed to dielectric barrier discharge (DBD)-generated plasma prior (e) and after annealing at 2073 K (f). The insets to (e) and (f) are detailed images of the HOPG substrate modified with the DBD-generated plasma before and after annealing at 2073, respectively. Imaging conditions: 0.2 nA (tunneling current) and 800 mV (bias voltage) (a), 0.3nA and 500 mV (c), 1.5nA and 5 mV (d), 1nA and 100mV (e,f).

View Article Online
DOI: 10.1039/C4NR05816J

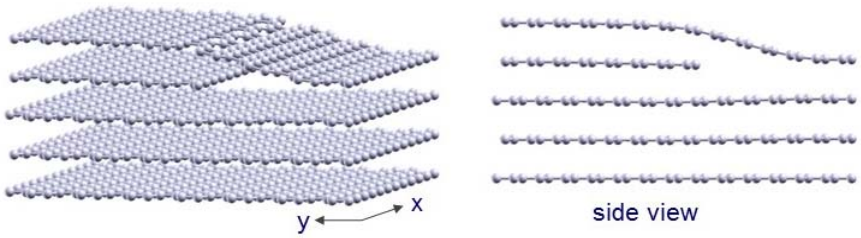

Figure 6 Relaxed structure of a graphene sheet covering two neighboring graphite terraces across a step edge. For clarity, only half of the simulation cell, containing one of the two step edges, is shown.

View Article Online
DOI: 10.1039/C4NR05816J

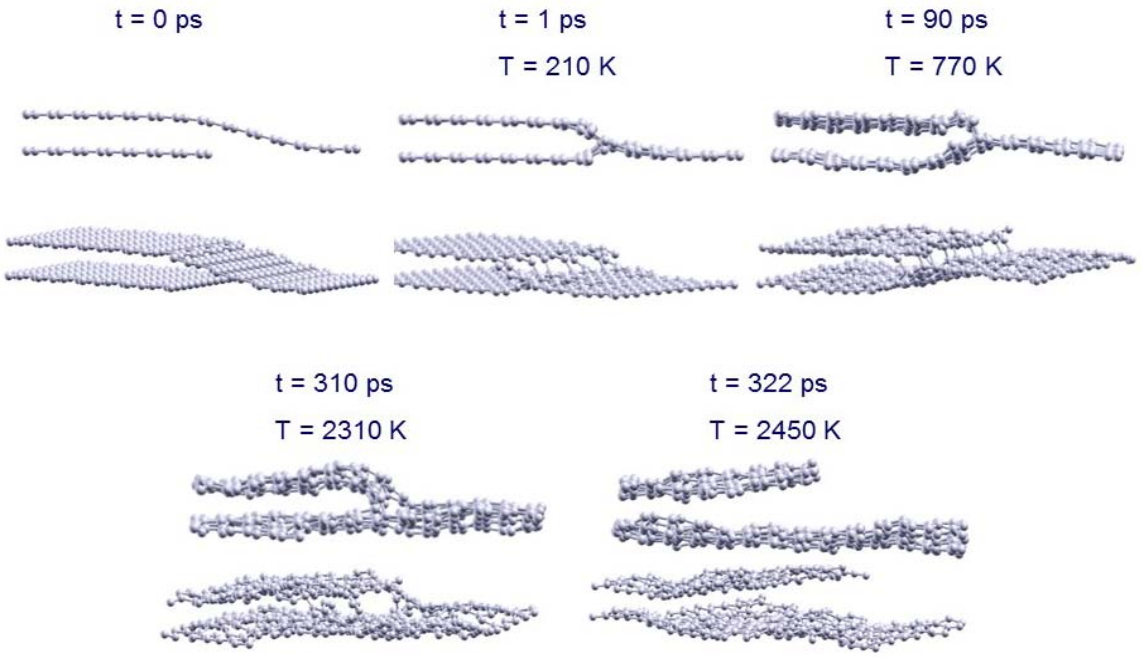

Figure 7 Side and perspective views of some snapshots taken along the dynamical simulations of the graphene sheet with a string of monatomic vacancies on top of the graphite step edge. For clarity, only half of the simulation cell and the two topmost layers, i.e. the graphene sheet with the string of vacancies and the upper terrace of the graphite surface, are shown.

View Article Online
DOI: 10.1039/C4NR05816J

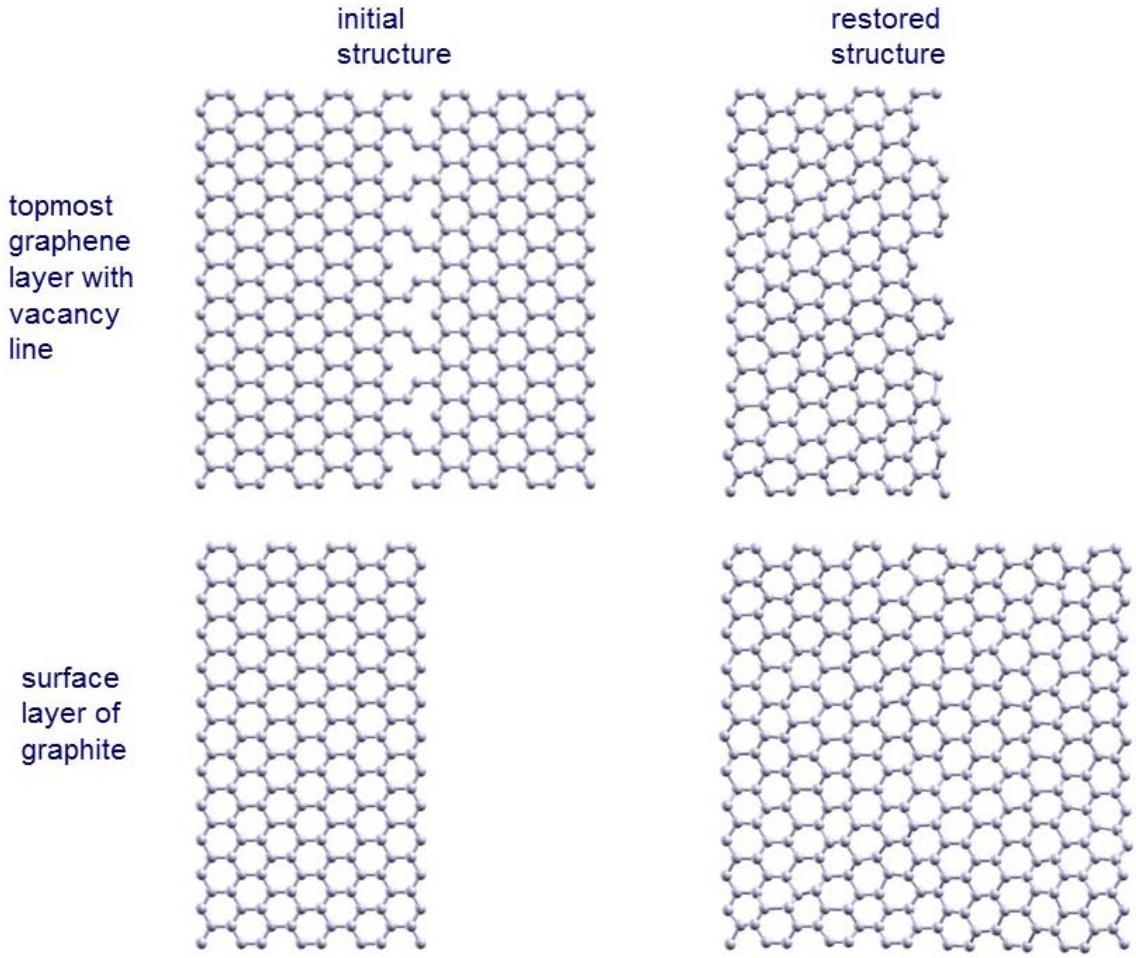

Figure 8 Top views of the initial and reconstructed structures of a graphene sheet decorated with a string of monatomic vacancies on top of the graphite step edge. For clarity, only the two topmost layers of the simulation, i.e. the graphene with the string of vacancies and the upper terrace of the graphite surface, are shown.

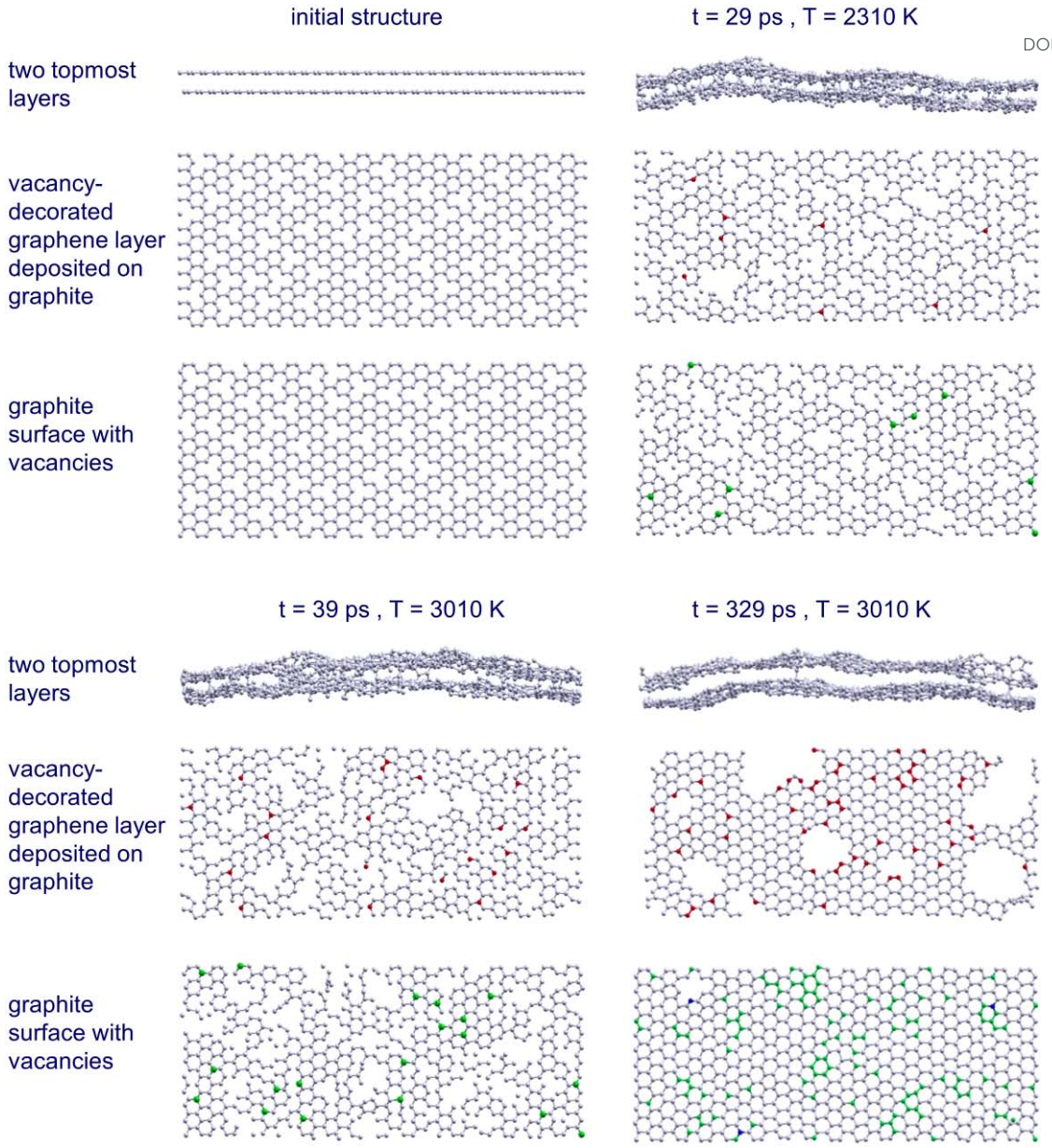

Figure 9 Side and top views of snapshots taken along the dynamical simulations of a vacancy-decorated graphene sheet deposited onto a vacancy-decorated graphite surface. Only the two topmost layers of the simulation, i.e. the two vacancy-decorated layers, are shown for clarity. Carbon atoms that originally belonged to the topmost graphene sheet but migrated to the underlying layer are represented in green, whereas carbon atoms that originally belonged to the surface layer of graphite and migrated to the graphene sheet are marked in red. A net migration of carbon atoms from the graphene sheet to the underlying graphite surface is observed, so that the latter is restored and large vacancies develop in the graphene sheet.